Polímeros
ISSN 1678-5169 (Online)

https://doi.org/10.1590/0104-1428.20210013

ORIGINAL ARTICLE

Modification of poly(lactic acid) filament with expandable graphite for additive manufacturing using fused filament fabrication (FFF): effect on thermal and mechanical properties

João Miguel Ayres Melillo[1], Iaci Miranda Pereira[2], Artur Caron Mottin[3*] and Fernando Gabriel da Silva Araujo[1]

[1]Rede Temática em Engenharia de Materiais – REDEMAT, Universidade Federal de Ouro Preto – UFOP, Ouro Preto, MG, Brasil

[2]Centro Tecnológico do Exército – CTEx, Rio de Janeiro, RJ, Brasil

[3]Departamento de Mecânica, Centro Federal de Educação Tecnológica de Minas Gerais – CEFET-MG, Belo Horizonte, MG, Brasil

**mottindesign@gmail.com*

Abstract

Fused Filament Fabrication, better known as Fused Deposition Modeling®, is currently the most widespread 3D Printing Technology. There has been a significant demand for developing flame-retardant filaments. Thereby enabling them, for example, in electronics and automotive applications. In this study, commercial PLA filament was modified by the addition of 1, 3 and 5% (%wt.) of expandable graphite. The composites were reprocessed, via extrusion, into filaments for Fused Filament Fabrication. Thermal properties of the filament composites were evaluated by thermogravimetric analysis and differential scanning calorimetry. Mechanical properties of thermo-pressed specimens indicated that no strong adhesion was promoted between the filler and matrix. This is a challenge with expandable graphite reported by many authors. All composites with expandable graphite achieved the V-2 rating of UL-94 flammability test. In spite of this, the results indicated that flammability of the PLA was reduced. All composite filaments were printable and prototypes were successfully 3D printed.

Keywords: *Fused Filament Fabrication (FFF), PLA, expandable graphite, prototypes.*

How to cite: Melillo, J. M. A., Pereira, I. M., Mottin, A. C., Araujo, F. G. S. (2021). Modification of poly(lactic acid) filament with expandable graphite for additive manufacturing using fused filament fabrication (FFF): effect on thermal and mechanical properties. *Polímeros: Ciência e Tecnologia, 31*(2), e2021024. https://doi.org/10.1590/0104-1428.20210013.

1. Introduction

Additive manufacturing (AM) alludes to adding raw materials during manufacturing, and includes several assembly and rapid prototyping processes[1]. Among the various AM technologies, material extrusion technology is currently the most popular[2,3]. Material extrusion technology was developed by Scott Crump in 1989 and patented as fused deposition modeling (FDM)[1]. Thus, FDM is the patented acronym and FFF is the "open-source" acronym for machines with the same principle, and stands for Fused Filament Fabrication. In FFF-type 3D printing a thermoplastic polymer filament undergoes melting-solidifying cycles before it forms a desirable shape, that is, only simple physical-state processes are involved[4]. Thus, it allows the user to print products of any dimension and complexity. In addition, the prototypes can be produced faster and customizable[4]. The most used thermoplastic polymers in FFF-type 3D printing are acrylonitrile butadiene styrene (ABS), poly(lactic acid) (PLA), high impact polystyrene (HIPS), thermoplastic polyurethane (TPU) and aliphatic polyamides (nylon)[5]. PLA is a bio-based polymer, that is, PLA is obtained from natural and sustainable raw material, such as cornstarch. Moreover, it degrades in soil by microorganisms under certain conditions of temperature and humidity[6]. In addition to these ecological benefits, PLA also offers reasonable performance in technical applications related to its mechanical properties[6]. However, its high ignitability is a drawback, since it limits the usage, for example, in electronics and automotive applications[7]. Therefore, there is a need to develop FFF materials with low flammability and density. Wang et al.[8], incorporated DOPO (9,10-dihydro9-oxa-10-phosphaphenanthrene-10-oxide) aminated derivative into PLA to improve the flame resistance. In spite of good results, higher content of DOPO-NH_2 presented uneven dispersion in PLA matrix, with decreasing in the mechanical properties. Xue et al. [9] developed a flame retardant poly(lactic acid) (PLA) composite with the addition of only 2 wt% of ammonium polyphosphate (APP)

and 0.12 wt% of resorcinol bis(diphenyl phosphate) (RDP). The composite achieved the V-0 rating of UL-94 test, with mechanical properties which enabled it to be drawn into filaments for FFF 3D printing. The use of natural graphite as flame retardant in polymers is limited by the difficulty of incorporation viscous polymers. Hence, for this usage it has been replaced with graphite treated with intercalation reagents, known as expandable graphite (EG)[10]. When EG composites are exposed to high temperature, EG expands and produces a voluminous protective layer, thus providing flame retardancy[10]. Wei et al.[11] used EG to produce fire retardant PLA. Their results indicated significant reduction at the rate of combustion due to the protective intumescent char created on the material surface. In this context, the main aim of this study was to modify 3D printing PLA filament with different contents of EG. The purpose of this is imparting flame-retardant property to the PLA filament. Moreover, prototypes made from the composite filaments were successfully 3D printed, which demonstrated that, in spite of modification, the filament kept printable.

2. Experimental

2.1 Materials

The white PLA filament was supplied by 3D LAB (Betim, MG). The expandable graphite (Grafexp 95200-110) was kindly donated by Nacional de Grafite (Itapericica, MG). Polyethylene glycol (PEG 20,000) was purchased from Sigma Aldrich (cod. 81300). All materials were used as received, without any further purification.

2.2 Modification of PLA filament with EG

First the EG was passed through a sieve (100 mesh) and then manually mixed and heated with PEG (T_m = 63-66 ºC). After cooling to room temperature, the mixture was ground (analytical mill IKA-A10). Three mixtures PEG/EG were prepared with different PEG: EG ratios (1:1, 1:3 and 1:5). After that, PLA filament was cut into pellets using a granulator (AX Plásticos - SP, Brazil). The pellets were manually premixed with each of the as prepared PEG/EG, in addition with the control PLA + PEG (without EG). Samples were named as PLA-EG0%, PLA-EG1%, PLA-EG3% and PLA-EG5% according to EG content. Composite Filaments with 1.75 mm diameter were obtained by extrusion at 180 °C using a mono-screw extruder (Filmaq3D STD - Brazil).

2.3 Plates production

To produce the plates the composite filaments were granulated and hot pressed (AX Plastics-AX P8T), at a temperature of 190 °C for 2 min under pressure of 2 t and an extra 2 min under pressure of 5 t. The plates were cut in specimens for the tensile test (ASTM D638), UL94 flammability assay and colorimetric assessment.

2.4 Characterizations

2.4.1 Scanning electron microscopy (SEM)

The morphology of EG before and after the thermal treatment at 900 ºC was observed using a scanning electron microscope (SEM, Bruker D2-phaser) with electron beam operating at 5kV.

2.4.2 Thermogravimetric analysis (TGA)

Thermogravimetric analysis was carried out in a DTA-60 thermoanalyzer (Shimatzu) under synthetic air atmosphere (flow = 50 mL min^{-1}). Five milligrams of each filament were placed in aluminum crucibles and the experiments were conducted from room temperature to 750 °C, using a heating rate of 10 °C min^{-1}.

2.4.3 Differential scanning calorimetry (DSC)

DSC analyses were performed in a differential scanning calorimeter PerkinElmer® DSC800 equipped with a PerkinElmer® Intracooler II standard and calibrated with high purity indium. Approximately two milligrams of each filament were placed in aluminum crucibles and the experiments were carried out under nitrogen atmosphere (flow = 20 mL min^{-1}). The following protocol was applied to each sample: (i) isotherm at -40 ºC for 3 min; (ii) heating from -40º C to 190 ºC, using heating rate of 30 ºC min^{-1}; (iii) isotherm at 190º C for 3.0 min; (iv) cooling from 190 ºC to -40 ºC, using cooling rate of 5º C $min^{-1;}$ (v) isotherm at -40 ºC for 3.0 min, and (vi) heating from -40 ºC to 190 ºC, using heating rate of 10 ºC min^{-1}.

The degree of crystallinity (χ_C) was estimated using Equation 1.

$$\chi_c = \frac{\Delta H_m - \Delta H_{cc}}{\Delta H_m^0 \times \left(1 - \frac{filler(\%w)}{100}\right)} \times 100 \quad (1)$$

Where ΔH_{CC} and ΔH_M are the enthalpies of cold crystallization and melting (J g^{-1}), respectively, which were calculated from the peaks of cold crystallization and melting in the DSC curves of the second heating. ΔH_m^0 = 93.1 J g^{-1} is the fusion enthalpy of 100% crystalline PLA[12], and filler (%w) is the weight percentage of EG.

2.4.4 Tensile test

Specimens cut according to ASTM D-638 (2014) were subjected to tensile tests using the universal testing machine (EMIC DL 2000) equipped with a 50 N load cell at a speed of 5 mm min^{-1}. For cutting the specimens, the filaments were pelleted and hot pressed (AX Plastics-AX P8T) at 190 °C for 2 min under 2 t pressure and another 2 min under 5 t pressure. The results presented are the average of at least three specimens with the standard deviation from the mean.

2.4.5 UL-94 vertical test

Composites flammability was preliminary assessed by the UL (Underwriter's Laboratory) 94 vertical burn test. UL-94 vertical test was carried out on strips measuring 125 mm × 13 mm × 3.0 mm following the ASTM D3801 standard. In this test, the upper part is clamped to a support and strips are ignited from the bottom, while the flame self-extinguishing time is measured (Figure 1).

The flame is brought into contact with the specimen for 10 s, after which the burner is removed and the flame self-extinguishing time is measured (T_1). The flame is brought once again into contact with the specimen for

10 s, and the flame self-extinguishing time is measured (T_2). The glow time (T_3) is measured after the application of the second flame, and the sum of after flame time and afterglow time is recorded, that is, T_2 plus T_3. At least five specimens for each sample were tested. The qualitative ranks for evaluating the test results are V-0, V-1, V-2 or non-rating[10,11,13]. Table 1 specifies the classification criteria used in the UL-94 vertical test.

From table 8.1 standard UL-94 Underwriters Laboratories Inc. revised July 29, 1997.

2.4.6 Colorimetry assay

The color parameters in the CIELab space were measured with the aid of a CM-600D spectrophotometer (Konica Minolta). The operating conditions of the spectrophotometer were: scanning from 360 to 740 nm, illuminating CIE D65 and observer angle of 10º. Five measurements were performed at different points of samples and the data were read by the Spectra Magic NX software. The parameters L*, a*, b*, as well as the color difference (ΔE*) in relation to the control (PLA-EG0%) were determined. The results were the average of the five values with the respective standard deviation.

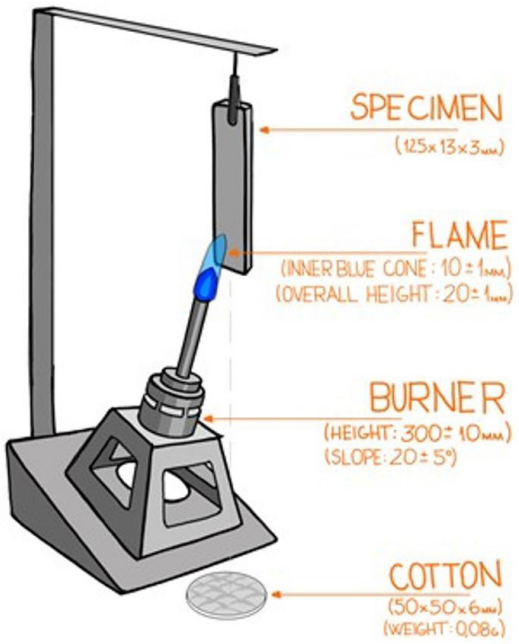

Figure 1. Vertical flame testing set.

2.5 FFF-type 3D printing

The 3D printing prototypes were fabricated using the composite filaments to feed a FFF-type 3D printer (Voolt 3D – Brazil) with a 0.30 mm nozzle. The nozzle and printing bed were heated to 190 °C and 65 °C, respectively. The layer height was set to 0.2 mm and a print speed of 50 mm/min was used. The computer aided design (CAD) was sourced from Thingiverse® (MakerBot Industries, LLC).

3. Results and discussion

3.1 Expandable graphite morphology

Expandable graphite (EG) is produced by inserting chemicals, such as sulfuric acid (H_2SO_4) or nitric acid (HNO_3), between the graphite layers[10]. When EG is exposed to high temperature, it expands due to releasing of gaseous products. A voluminous protective layer is produced, thus providing flame retardancy performance to various polymeric matrices[10]. The expansion of EG was carried out at 900 °C in a refractory oven for one minute. From the ratio between density and volume it was possible to verify that, after the heat treatment the graphite density decreased 9 times. Figure 2 shows SEM images of EG before and after the heat treatment.

3.2 Thermal behavior of composite filaments

In FDM 3D printers the filament passes it through a high temperature nozzle where it is heated to a soft state. So, it is important a previous knowledge about their thermal properties.

3.2.1 Thermogravimetric analysis (TGA)

For all filaments the onset of degradation occurs just above 260 °C (curves not shown). There was no significant difference in thermal stability between them. Yang et al. [14] indicated the temperature of 326 °C as the beginning of PLA degradation. However, these authors also realized that when PEG is added to PLA, the thermal stability was reduced due to the poor thermal stability of PEG. Liu et al. [15] reported that the addition of 5% PEG 6000 shifted the TG curve to lower temperatures compared to that of pristine PLA. The same was observed by us, probably denoting lack of adhesion between phases, with possible PEG segregation.

Table 2 shows the values from DTG curves (not shown).

The peaks at T_1 and T_2 were associated with polymer degradation. It can be noted that in the composite filaments the first peak at T_1 appeared at temperatures well below that of PLA-EG0%.

Table 1. Ratings of UL 94 vertical test.

Criteria conditions	V0	V1	V2
Afterflame time for each individual specimen t1 or t2	≤10 s	≤30 s	≤30 s
Total afterflame time for any condition set (t1 plus t2 for the 5 specimens)	≤50 s	≤250 s	≤250 s
Afterflame plus afterglow time for each individual specimen after the second flame application (t2+t3)	≤30 s	≤60 s	≤60 s
Afterflame or afterglow of any specimen up to the holding clamp	No	No	No
Cotton indicator ignited by flaming particles or drops	No	No	Yes

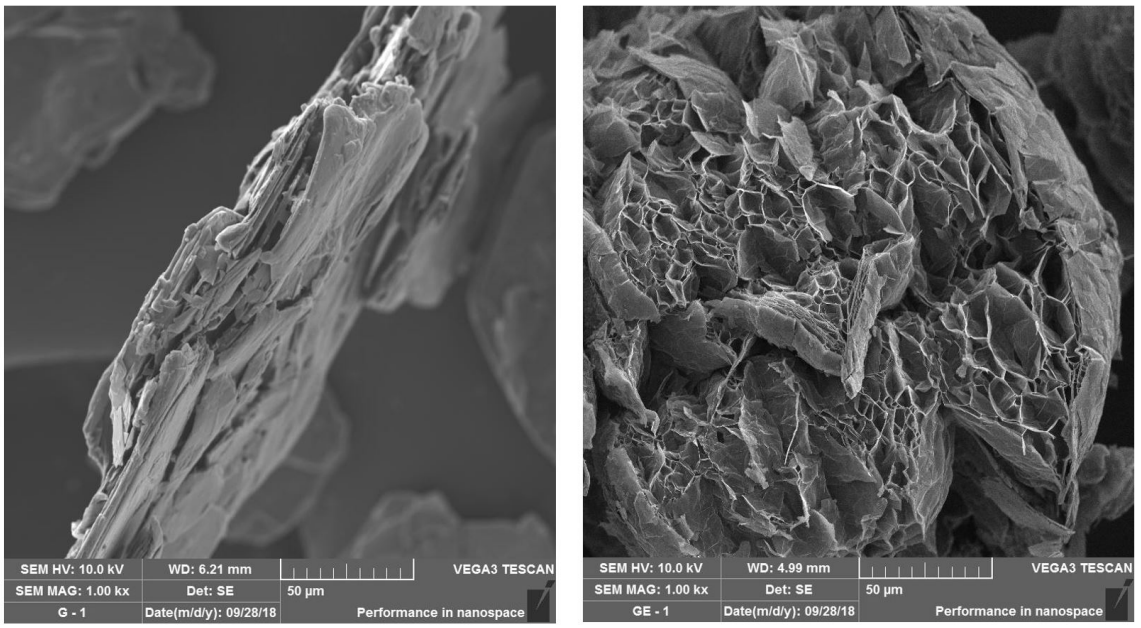

Figure 2. SEM images of EG before (left) and after (right) the heat treatment.

Table 2. Results of TGA obtained from DTG curves.

Filament	$T_{1max\ deg}$ (°C)	$T_{2max\ deg}$ (°C)	$T_{3max\ deg}$ (°C)	Residue
PLA-EG0%	363		502	
PLA-EG1%	341	365	502	
PLA-EG3%	343	369	492	
PLA-EG5%	335	360	489	1.15

Tmax deg: temperature at which maximum degradation occurs.

Probably, T_1 for the composites had suffered interference from EG expansion, starting at 280 °C, in which sulfuric acid is released from confinement with formation of volatiles[11], promoting reduction in the molar mass of PLA[16]. After this, the composites show the same temperature range (T_2) of PLA-EG0%.

In addition, it is possible to perceive the effect of EG in increasing thermal stability, when the maximum degradation temperature goes from 363 to 365 and then to 369 °C, as the EG content increases. This behavior is the same observed by several authors and is attributed to the barrier effect promoted by EG due to the swelling that occurs after exfoliation[17].

However, the filament with the highest EG content showed the lowest thermal stability, with $T_{deg\ max}$ below PLA-EG0%. Uhl et al.[17] found slightly increase in the maximum temperature of degradation at 1% EG, while high expandable graphite contents, 3% and 5%, apparently were detrimental to PA-6 stability. They attributed this to the release of acid degradation products, which could facilitate the degradation of the PA-6. The peak at T_3 is due to reaction with oxygen and carbonization of the samples[18].

3.2.2 Differential scanning calorimetry (DSC)

Usually, DSC analysis involves three steps. The first heating to erase the polymer thermal history. The thermal history refers to the heating / cooling processes to which the sample was submitted, prior to carrying out the thermal analysis[19]. The cooling to assess the ability of the polymer to crystallize under cooling. And finally, a second heating to check the crystallization under heating, if any, in addition to melting and second order transitions, such as glass transition temperature.

It was not possible to observe the crystallization of PLA during cooling in any of the compositions. Athanasoulia et al. [20] did not observe crystallization peak during the cooling (10 °C min^{-1}) of pristine PLA. According to them, this fact is due to the highly amorphous nature of PLA. By using a cooling rate of 5 °C min^{-1} they were able to visualize a small and large crystallization peak around 95 °C. In our case, even with slow cooling at 5 ºC min^{-1}, it was not possible to visualize any exothermic event corresponding to PLA crystallization. Refaa et al.[21] studied PLA crystallization PLA in detail. According to them, during PLA crystallization the cooling kinetics exceeds the crystallization kinetics. Thus, for cooling rates greater than 2 ºC min^{-1} the obtained PLA is practically amorphous.

Li and Huneault[22] also reported that they did not observe the exothermic peak referring to pristine PLA cooling crystallization (20 ºC min^{-1}). According to these authors, the addition of PEG enhances the mobility of PLA chains

facilitating crystallization during cooling. However, even with 5% PEG (3350 g mol^{-1}) they were unable to detect the crystallization. Only with PEG content above 10%, such authors reported a wide and weak crystallization exotherm around 80 ºC. In view of this, it is reasonable to think that with a content of 1% PEG, as in our case, it would be hard to visualize the crystallization exotherm during cooling.

Figure 3 shows the DSC curves obtained in the second heating. The values represent the average of two samples.

Table 3 summarizes the parameters collected from DSC second heating.

The glass transition temperature of PLA and the melting temperature of PEG are very close, and can easily overlap[23]. The event that appears around 60 ºC was treated as Tg of the PLA. According to the values in Table 3, Tg slightly increased with EG content up to 3%, but it was not visualized for higher EG content. Possibly due to a reduction in the amount of PLA amorphous phase[20]. In contrast, Mngomezulu et al. [18] observed a slight steadily increase in Tg of PLA for EG content of 5, 10 and 15%.

In the case of PLA, which is a predominantly amorphous polymer, but crystallizable, cold crystallization can occur during heating[24]. Conversely, if PEG does not completely crystallize during cooling, it will not crystallize during subsequent heating[25]. Athanasoulia et al.[26] reported that the cold crystallization peak of PLA disappeared when the cooling rate was lowered from 10 °C min^{-1} to 2 °C min^{-1}. They attributed this to the completion of crystallization process during cooling, due to the low cooling rate used.

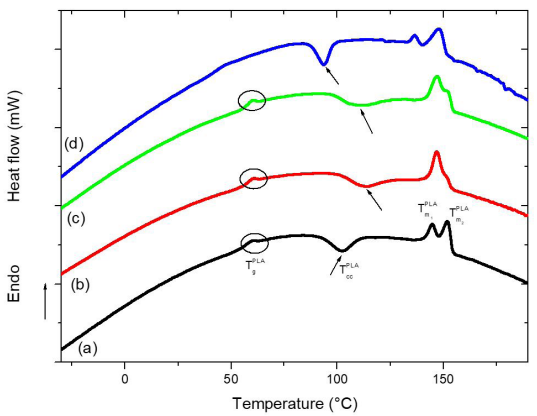

Figure 3. DSC curves obtained from second heating: (a) PLA-EG0%, (b) PLA-EG1%, (c) PLA-EG3% and (d) PLA-EG5%.

All DSC curves in Figure 3 exhibited cold crystallization upon heating. In respect to PLA-EG0% (Table 3), cold crystallization temperature (T_{cc}) was shifted to lower value than T_{cc} reported for pristine PLA. This behavior is usually attributed to the plasticizing effect of PEG[26]. With the addition of 1% EG T_{cc} increased of about 10 ºC, but T_{cc} shifted to lower values for higher EG contents.

Barletta et al.[27] reported that better homogeneity and stronger interactions give rise to composites with larger interfacial area between polymer and filler. At this interface, the filler can effectively decrease the free energy of arising new crystalline nuclei and, therefore, increase the trend of polymer to crystallize during heating (T_{cc} decreases). Murariu et al.[28] attested the nucleating effect of expanded graphite in PLA composites. They observed the shift of T_{cc} to lower temperatures compared with T_{cc} of pristine PLA.

On the other hand, stronger interactions between matrix and filler might also act in the opposite direction, reducing the mobility of polymer chains and, therefore, their ability in relation to rearrangement in ordered crystalline structures (T_{cc} increases)[22]. In our case, the behavior of cold crystallization seems to be related to the EG content. T_{cc} increased in PLA- EG1% and PLA- EG3%, probably due to strong interactions between EG and matrix which would be hindering cold crystallization. Conversely, T_{cc} decreased in PLA- EG5%, possibly due to EG action as nucleating agent.

Regarding the degree of crystallinity (Table 3), all samples containing EG presented higher degree of crystallinity (χ_c) than PLA-EG0%. However, χ_c slightly decreased in PLA-EG5% compared with PLA-EG3%. Murariu et al.[28] reported low χ_c, around 1%, for pristine PLA. According to them, addition of expanded graphite up to 6% resulted in a pronounced increase of χ_c. For further nanofiller addition authors observed a reduction in χ_c. They attributed this fact to possible aggregation of the graphite.

The curves of Figure 3 show a double melting peak, which is usually associated with the melting of crystals of different sizes and shapes[18]. There are also some studies relating double melting peak with the recrystallization of the melt during the second heating cycle[21]. Androsch et al.[29] described the conditions under disordered PLA α' crystals could recrystallize into more stable PLA α crystals. However, they reported melting temperature of α crystals around 170-180 ºC, far above melting temperatures found by us. The curves in Figure 3 showed different ratios of areas between the two melting peaks. Refaa et al.[21] related such difference with different heating rates. In our case, there was no variation in the heating rate.

Table 3. Data from DSC second heating.

Filament	T_g^{PLA} (°C)	T_{cc}^{PLA} (°C)	ΔH_{cc} (J/g)	T_{m1}^{PLA} (°C)	T_{m2}^{PLA} (°C)	ΔH_m (J/g)	χ_c (%)
PLA-EG0%	59.0	102.3	-13.26	144.8	151.9	15.71	2.6
PLA-EG1%	60.3	112.0	-11.56	146.8	151.8	18.68	7.7
PLA-EG3%	60.5	111.1	-12.34	147.1	152.0	20.09	8.6
PLA-EG5%		94.0	-17.52	137.0	148.3	25.02	8.5

T_g^{PLA}: PLA glass transition temperature, T_{cc}^{PLA}: PLA cold crystallization temperature, ΔH_{cc}: cold crystallization enthalpy, T_m^{PLA}: PLA melting temperature, ΔH_m: melting enthalpy and χ_c: crystallinity degree.

3.3 Tensile properties

The values of mechanical properties derived from the tensile test are shown in Table 4.

As can be seen in Table 4, tensile strength diminished as EG content increased. Yang et al.[30] reported that, with 5% of bio-based flame retardant, both tensile strength and elongation at break were negatively affected. According to them, probably due to adverse impacts on the crystallization and molar mass of PLA. In fact, the DSC results indicated that addition of EG might be affecting the crystallization behavior of PLA. On the other hand, Li et al.[31] stated that the poor interfacial compatibility between EG and the polymer results in an outstanding decrease in the polymer mechanical properties. To overcome this shortcoming, such authors suggested decreasing the particle size of EG and adding octene–ethylene (POE). Even though, the tensile strength kept decreasing with increasing of POE content.

The increase in Young's modulus was only noticeable in PLA-EG5%. Similar behavior was also observed for PA 11 composites reinforced with expandable graphite[32].

Maybe the graphite particles incorporated into the PLA fracture before the sample breaks or have very little adhesion to the matrix and are pulled out of the matrix[33]. Likewise, the elongation at break decreased whereas the modulus increased as EG content increased. This behavior can be justified by the low tensile deformation capacity of graphite, below 0.5%, and high value of the Young's modulus of graphite (4100 MPa to 27,000 MPa), respectively[33].

3.4 Vertical burning test (UL-94)

The results of ranking criteria (see Table 1) is shown in Table 5.

Only PLA-EG0% did not achieve classification according to the criteria for UL-94 test. All composites presented burning the cotton by dripping the material in flames or sparks emitted. Otherwise, composites with 1% and 3% graphite would be classified as V-1 and the composite with 1% graphite would be classified as V-0. Wei, Bocchini and Camino[11] reported that pristine PLA was not classified as a flame retardant, since it completely burned with flaming drip. Herein, PLA-EG0% had the same behavior and did not obtain classification in the UL-94 test. For composite with 1 wt. % of expansible graphite, combustion time was reduced, but authors reported flaming dripping. They classified the composites as V-2, the same level of ours. However, unlike us, with 5 wt. % of EG, they reached level V-0. Two hypotheses are suggested to justify this disagreement. The first is that the presence of PEG might be impairing the performance of EG as flame retardant. However, It was already demonstrated the synergism between PEG and ammonia polyphosphate (APP) in the system PLA / PEG 20,000 / APP to obtain the V-0 classification[34]. Thus, there is not an objective evidence to support the hypothesis that the presence of PEG may be responsible for PLA-EG5% composite not reaching the V-0 classification.

The second hypothesis is that the lack of adhesion between the phases might be responsible for the poor performance of EG. According to Chen et al.[35], the lack of compatibility between the polymer matrix and the expandable graphite impairs the performance of this flame retardant. Mngomezulu et al.[18] observed that graphite layers were still aggregated and with poor filler dispersion in PLA matrix.

Conforming to Li et al.[36], the addition of silane coupling agent gave rise to grafted EG (GEG). Both, the dispersion and the compatibility with the matrix of low-density polyethylene were improved. The effect as flame retardant of GEG (UL-94 V-0) was achieved with content of approximately 12 and 15 wt. %. Xiong et al.[37] also attributed better thermal stability and flame-resistance in poly (urethane-imide) (PUI)/EG foams to silane coupling agent.

3.5 Colorimetry assay

Color representation systems translate the colors of objects by numbers. The CIELAB space is composed of three axes. The vertical L* axis represents lightness and varies from 100 (white) to zero (black). The a* and b* axes represent chromacity. The a* axis varies from +a* (red) to –a* (green). The b* axis varies from + b* (yellow) to –b* (blue)[38]. The color difference between two stimuli, the standard and the sample, can be quantified in the diagram L* a* b*. The distance between the two positions, that is, the total color change (ΔE*), is defined by Equation 2[38].

Table 4. Values of tensile properties.

Specimen	σ (MPa)	ε (%)	E (MPa)
PLA-EG0%	34.03 ± 1.01	20.94 ± 1.29	727 ± 15.5
PLA-EG1%	29.72 ± 3.94	20.71 ± 1.20	731 ± 16.4
PLA-EG3%	23.73 ± 0.12	18.59 ± 0.08	733 ± 4.50
PLA-EG5%	4.70 ± 1.62	16.38 ± 0.86	830 ± 38.0

σ: tensile strength, ε: elongation at break and E: Young modulus.

Table 5. Classification in the test for flammability (UL-94).

Sample	T_1	T_2	T_1+T_2	T_2+T_3	Flaming particles	Classification
PLA-EG0%	<10	***	<250	***	Yes	None
PLA-EG1%	<30	<30	<50	<60	Yes	V-2
PLA-EG3%	<30	<30	<250	<60	Yes	V-2
PLA-EG5%	<10	<10	<50	<30	Yes	V-2

T = time in seconds. *** not applicable.

$$\Delta E^* = \sqrt{\left(\Delta L^*\right)^2 + \left(\Delta a^*\right)^2 + \left(\Delta b^*\right)^2} \quad (2)$$

The values of L*, a* and b*, along with the values of ΔE* and A (absorbance), for PLA-EG0% (standard) and their composites with EG are shown in Table 6.

The absorbance behaved as expected, that is, it increased steadily with EG content. This trend is in line with the results found by Przekop et al.[33]. The authors' research involved addition of graphite into PLA to produce filaments. According to criteria reported by these authors, the ΔE* value of PLA-EG1% can already be classified as marked color difference compared to PLA-EG0%. Obviously, ΔE* value increases with the increase in EG content.

4. Prototypes additively manufactured using FFF-type 3D printer

In FFF technology, the thermoplastic polymer filament is driven to an extruder that contains a heater to melt it. The filament is pulled inward with the aid of a roller mechanism in the feeder and extruded the molten polymer through a circular nozzle. The nozzle extrudes semi liquid-state filament and laid it to desired location with the help of the programmed tri-axial actuator. The 3D printed part is formed on a flat surface platform, known as heat bed[4,39].

Figure 4 shows the obtained composite filaments and the FFF-type 3D printer used to additively manufacture of the prototypes (in detail).

Since 3D printing process is performed in layers, the part has an evident marking of the layers. To circumvent this effect and reduce the visible "steps", the layer height might be reduced. This adjustment improves the surface quality of the part, but the time needed to print considerably increases[40]. A manner to let the part with finer finish is to carry out a post treatment. Different methods include the use of chemical solutions, heat, laser and ultrasound. The most common chemical used to reduce the surface roughness is acetone. However, PLA is not so easily dissolved in acetone, which makes it difficult to smooth the layers[41]. Although several challenges and limitations exist, additive manufacturing

Table 6. CIELAB parameters, total color variation (ΔE *) and absorbance (A).

Sample	L*	a*	b*	ΔE*	A
PLA-EG0%	81.34±2.03	-2.15±0.09	4.66±0.32		0.3±0.01
PLA-EG1%	43.13±1.23	-0.72±0.07	-2.24±0.23	38.85±1.23	0.84±0.02
PLA-EG3%	31.88±1.07	-0.29±0.04	-1.77±0.25	49.90±1.04	1.11±0.03
PLA-EG5%	27.69±0.51	-0.14±0.05	-1.58±0.22	54.04±0.52	1.23±0.01

Absorbance at 420 nm.

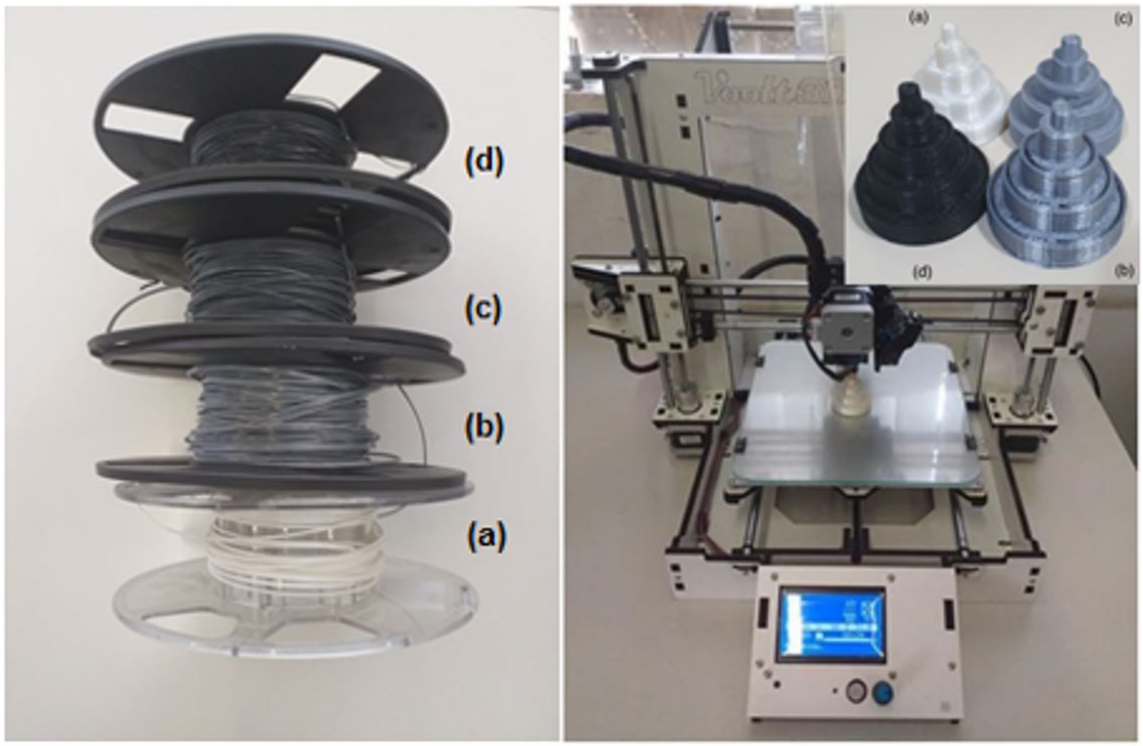

Figure 4. Prototypes additively manufactured using FFF-type 3D printer fed with: (a) PLA-EG0%, (b) PLA-EG1%, (c) PLA-EG3% and (d) PLA-EG5%.

(AM) is expected to revolutionize the fabrication process of engineering components[1].

5. Conclusions

The possibility of printing parts with complex shapes, with the exact amount of raw material, is a great advantage of 3D printing. In this study, composite filaments based on PLA and 1, 3 and 5 wt.% of EG were developed for using in FFF-type 3D printing. The effect of EG on thermal and tensile properties of PLA was investigated. Based on the findings of these analyses, it is likely that expandable graphite needs stronger interfacial adhesion with the PLA matrix. The possibility to impart anti-flammability property to PLA filament by modifying it with expansible graphite was evaluated. All composites reached the classification V-2 in the vertical burning test (UL-94). This was not the expected result, and it's probably due to the lack of adhesion between phases, as pointed out by the mechanical and thermal assays. The obtained composite filaments kept printable, and prototypes were successfully made from all of them. Further research should involve silane as coupling agent and also a flame co-retardant to work in synergism with expansible graphite.

6. Acknowledgements

The authors acknowledge the financial support from National Council for Scientific and Technological Development - CNPq and National Council for Scientific and Technological Development Coordination for the Improvement of Higher Education Personnel – CAPES. The authors would also like to acknowledge Nacional de Grafite for kindly supplying expansible graphite.

7. References

1. Khosravani, M. R., & Reinicke, T. (2020). On the environmental impacts of 3D printing technology. *Applied Materials Today*, *20*, 100689. http://dx.doi.org/10.1016/j.apmt.2020.100689.
2. Wu, H., Sulkis, M., Driver, J., Saade-Castillo, A., Thompson, A., & Koo, J. H. (2018). Multi-functional ULTEM™1010 composite filaments for additive manufacturing using Fused Filament Fabrication (FFF). *Addittive Manufecturing*, *24*, 298-306. http://dx.doi.org/10.1016/j.addma.2018.10.014.
3. Singh, S., Ramakrishna, S., & Berto, F. (2020). 3D Printing of polymer composites: a short review. *Material Design & Processing Communications*, *2*(2), e97. http://dx.doi.org/10.1002/mdp2.97.
4. Seng, C. T., A/L Eh Noum, S. Y., A/L Sivanesan, S. K. & Yu, L.-J. (2020). Reduction of hygroscopicity of PLA filament for 3D printing by introducing nano silica as filler. *AIP Conference Proceedings*, *2233*(1), 020024. https://doi.org/10.1063/5.0001927.
5. Lee, K. M., Park, H., Kim, J., & Chun, D. M. (2019). Fabrication of a superhydrophobic surface using a fused deposition modeling (FDM) 3D printer with poly lactic acid (PLA) filament and dip coating with silica nanoparticles. *Applied Surface Science*, *467*, 979-991. http://dx.doi.org/10.1016/j.apsusc.2018.10.205.
6. Maqsood, M., & Seide, G. (2020). Biodegradable Flame Retardants for Biodegradable *Polymer. Biomolecules*, *10*(7), 1038. http://dx.doi.org/10.3390/biom10071038. PMid:32664598.
7. Chow, W. S., Teoh, E. L., & Karger-Kocsis, J. (2018). Flame retarded poly (lactic acid): A review. *Express Polymer Letters*, *12*(5), 396-417. http://dx.doi.org/10.3144/expresspolymlett.2018.34.
8. Wang, X., He, W., Long, L., Huang, S., Qin, S., & Xu, G. (2020). A phosphorus-and nitrogen-containing DOPO derivative as flame retardant for polylactic acid (PLA). *Journal of Thermal Analysis and Calorimetry*, *145*(2), 331-343. http://dx.doi.org/10.1007/s10973-020-09688-7.
9. Xue, Y., Zuo, X., Wang, L., Zhou, Y., Pan, Y., Li, J., Yin, Y., Li, D., Yang, R., Rafailovich, M. H., & Guo, Y. (2020). Enhanced flame retardancy of poly (lactic acid) with ultra-low loading of ammonium polyphosphate. *Composites. Part B, Engineering*, *196*, 108124. http://dx.doi.org/10.1016/j.compositesb.2020.108124.
10. Babu, K., Rendén, G., Afriyie Mensah, R., Kim, N. K., Jiang, L., Xu, Q., Restás, Á., Esmaeely Neisiany, R., Hedenqvist, M. S., Försth, M., Byström, A., & Das, O. (2020). A review on the flammability properties of carbon-based polymeric composites: state-of-the-art and future trends. *Polymers*, *12*(7), 1518. http://dx.doi.org/10.3390/polym12071518. PMid:32650531.
11. Wei, P., Bocchini, S., & Camino, G. (2013). Flame retardant and thermal behavior of polylactide/expandable graphite composites. *Polimery*, *58*(5), 361-364. http://dx.doi.org/10.14314/polimery.2013.361.
12. Brisigueli, R. P., & Morales, A. R. (2014). Study of mechanical and thermal behavior of pla modified with nucleating additive and impact modifier. *Polímeros: Ciência e Tecnologia*, *24*(2), 198-202. http://dx.doi.org/10.4322/polimeros.2014.042.
13. Jang, J., & Lee, E. (2000). Improvement of the flame retardancy of paper-sludge/polypropylene composite. *Polymer Testing*, *20*(1), 7-13. http://dx.doi.org/10.1016/S0142-9418(99)00072-0.
14. Yang, Y., Haurie, L., Wen, J., Zhang, S., Ollivier, A., & Wang, D. Y. (2019). Effect of oxidized wood flour as functional filler on the mechanical, thermal and flame-retardant properties of polylactide biocomposites. *Industrial Crops and Products*, *130*, 301-309. http://dx.doi.org/10.1016/j.indcrop.2018.12.090.
15. Liu, C., Ye, S., & Feng, J. (2017). Promoting the dispersion of graphene and crystallization of poly (lactic acid) with a freezing-dried graphene/PEG masterbatch. *Composites Science and Technology*, *144*, 215-222. http://dx.doi.org/10.1016/j.compscitech.2017.03.031.
16. Acuña, P., Li, Z., Santiago-Calvo, M., Villafañe, F., Rodríguez-Perez, M. Á., & Wang, D. Y. (2019). Influence of the characteristics of expandable graphite on the morphology, thermal properties, fire behaviour and compression performance of a rigid polyurethane foam. *Polymers*, *11*(1), 168. http://dx.doi.org/10.3390/polym11010168. PMid:30960151.
17. Uhl, F. M., Yao, Q., Nakajima, H., Manias, E., & Wilkie, C. A. (2005). Expandable graphite/polyamide-6 nanocomposites. *Polymer Degradation & Stability*, *89*(1), 70-84. http://dx.doi.org/10.1016/j.polymdegradstab.2005.01.004.
18. Mngomezulu, M. E., Luyt, A. S., & John, M. J. (2019). Morphology, thermal and dynamic mechanical properties of poly (lactic acid)/expandable graphite (PLA/EG) flame retardant composites. *Journal of Thermoplastic Composite Materials*, *32*(1), 89-107. http://dx.doi.org/10.1177/0892705717744830.
19. Bannach, G., Perpétuo, G. L., Cavalheiro, E. T. G., Cavalheiro, C. C. S., & Rocha, R. R. (2011). Effects of the thermal history on thermal properties of polymers: an experiment for thermal analysis education. *Quimica Nova*, *34*(10), 1825-1829. http://dx.doi.org/10.1590/S0100-40422011001000016.
20. Athanasoulia, I. G. I., Christoforidis, M. N., Korres, D. M., & Tarantili, P. A. (2019). The effect of poly(ethylene glycol)mixed with poly(L-lactic acid) on the crystallization characteristics and properties of their blends. *Polymer International*, *68*(4), 788-804. http://dx.doi.org/10.1002/pi.5769.

21. Refaa, Z., Boutaous, M. H., Xin, S., & Siginer, D. A. (2017). Thermophysical analysis and modeling of the crystallization and melting behavior of PLA with talc. *Journal of Thermal Analysis and Calorimetry*, *128*(2), 687-698. http://dx.doi.org/10.1007/s10973-016-5961-1.
22. Li, H., & Huneault, M. A. (2007). Effect of nucleation and plasticization on the crystallization of poly (lactic acid). *Polymer*, *48*(23), 6855-6866. http://dx.doi.org/10.1016/j.polymer.2007.09.020.
23. Li, F. J., Zhang, S. D., Liang, J. Z., & Wang, J. Z. (2015). Effect of polyethylene glycol on the crystallization and impact properties of polylactide-based blends. *Polymers for Advanced Technologies*, *26*(5), 465-475. http://dx.doi.org/10.1002/pat.3475.
24. Ortenzi, M. A., Basilissi, L., Farina, H., Di Silvestro, G., Piergiovanni, L., & Mascheroni, E. (2015). Evaluation of crystallinity and gas barrier properties of films obtained from PLA nanocomposites synthesized via "*in situ*" polymerization of l-lactide with silane-modified nanosilica and montmorillonite. *European Polymer Journal*, *66*, 478-491. http://dx.doi.org/10.1016/j.eurpolymj.2015.03.006.
25. Hu, Y., Hu, Y. S., Topolkaraev, V., Hiltner, A., & Baer, E. (2003). Crystallization and phase separation in blends of high stereoregular poly (lactide) with poly (ethylene glycol). *Polymer*, *44*(19), 5681-5689. http://dx.doi.org/10.1016/S0032-3861(03)00609-8.
26. Athanasoulia, I.-G., Giachalis, K., Todorova, N., Giannakopoulou, T., Tarantili, P., & Trapalis, C. (2021). Preparation of hybrid composites of PLLA using GO/PEG masterbatch and their characterization. *Journal of Thermal Analysis and Calorimetry*, *143*(5), 3385-3399. http://dx.doi.org/10.1007/s10973-019-09227-z.
27. Barletta, M., Pizzi, E., Puopolo, M., Vesco, S., & Daneshvar-Fatah, F. (2017). Thermal behavior of extruded and injection-molded poly (lactic acid)–talc engineered biocomposites: effects of material design, thermal history, and shear stresses during melt processing. *Journal of Applied Polymer Science*, *134*(32), 45179. http://dx.doi.org/10.1002/app.45179.
28. Murariu, M., Dechief, A. L., Bonnaud, L., Paint, Y., Gallos, A., Fontaine, G., Bourbigot, S., & Dubois, P. (2010). The production and properties of polylactide composites filled with expanded graphite. *Polymer Degradation & Stability*, *95*(5), 889-900. http://dx.doi.org/10.1016/j.polymdegradstab.2009.12.019.
29. Androsch, R., Zhang, R., & Schick, C. (2019). Melt-recrystallization of poly (L-lactic acid) initially containing α′-crystals. *Polymer*, *176*, 227-235. http://dx.doi.org/10.1016/j.polymer.2019.05.052.
30. Yang, Y. X., Haurie, L., Zhang, J., Zhang, X. Q., Wang, R., & Wang, D. Y. (2020). Effect of bio-based phytate (PA-THAM) on the flame retardant and mechanical properties of polylactide (PLA). *Express Polymer Letters*, *14*(8), 705-716. http://dx.doi.org/10.3144/expresspolymlett.2020.58.
31. Li, R., Wang, N., Bai, Z., Chen, S., Guo, J., & Chen, X. (2021). Microstructure design of polypropylene/expandable graphite flame retardant composites toughened by the polyolefin elastomer for enhancing its mechanical properties. *RSC Advances*, *11*(11), 6022-6034. http://dx.doi.org/10.1039/D0RA09978C.
32. Oulmou, F., Benhamida, A., Dorigato, A., Sola, A., Messori, M., & Pegoretti, A. (2019). Effect of expandable and expanded graphites on the thermo-mechanical properties of polyamide 11. *Journal of Elastomers and Plastics*, *51*(2), 175-190. http://dx.doi.org/10.1177/0095244318781956.
33. Przekop, R. E., Kujawa, M., Pawlak, W., Dobrosielska, M., Sztorch, B., & Wieleba, W. (2020). Graphite modified polylactide (PLA) for 3D printed (FDM/FFF) sliding elements. *Polymers*, *12*(6), 1250. http://dx.doi.org/10.3390/polym12061250. PMid:32486090.
34. Sun, Y., Sun, S., Chen, L., Liu, L., Song, P., Li, W., Yu, Y., Fengzhu, L., Qian, J., & Wang, H. (2017). Flame retardant and mechanically tough poly (lactic acid) biocomposites via combining ammonia polyphosphate and polyethylene glycol. *Composites Communications*, *6*, 1-5. http://dx.doi.org/10.1016/j.coco.2017.07.005.
35. Chen, C. H., Yen, W. H., Kuan, H. C., Kuan, C. F., & Chiang, C. L. (2010). Preparation, characterization, and thermal stability of novel PMMA/expandable graphite halogen-free flame-retardant composites. *Polymer Composites*, *31*(1), 18-24. http://dx.doi.org/10.1002/pc.20787.
36. Li, L., Wang, D., Chen, S., Zhang, Y., Wu, Y., Wang, N., Chen, X., Qin, J., Zhang, K., & Wu, H. (2020). Effect of organic grafting expandable graphite on combustion behaviors and thermal stability of low-density polyethylene composites. *Polymer Composites*, *41*(2), 719-728. http://dx.doi.org/10.1002/pc.25401.
37. Xiong, W., Liu, H., Tian, H., Wu, J., Xiang, A., Wang, C., Ma, S., & Wu, Q. (2020). Mechanical and flame-resistance properties of polyurethane-imide foams with different-sized expandable graphite. *Polymer Engineering and Science*, *60*(9), 2324-2332. http://dx.doi.org/10.1002/pen.25475.
38. Pagnan, C. S., Mottin, A. C., Oréfice, R. L., Ayres, E., & Câmara, J. J. D. (2018). Annatto-colored poly (3-hydroxybutyrate): a comprehensive study on photodegradation. *Journal of Polymers and the Environment*, *26*(3), 1169-1178. http://dx.doi.org/10.1007/s10924-017-1026-1.
39. Subramaniam, S. R., Samykano, M., Selvamani, S. K., Ngui, W. K., Kadirgama, K., Sudhakar, K., & Idris, M. S. (2019). 3D printing: overview of PLA progress. *AIP Conference Proceedings*, *2059*(1), 020015. https://doi.org/10.1063/1.5085958.
40. Pérez, M., Medina-Sánchez, G., García-Collado, A., Gupta, M., & Carou, D. (2018). Surface quality enhancement of fused deposition modeling (FDM) printed samples based on the selection of critical printing parameters. *Materials (Basel)*, *11*(8), 1382. http://dx.doi.org/10.3390/ma11081382. PMid:30096826.
41. Wickramasinghe, S., Do, T., & Tran, P. (2020). FDM-based 3D printing of polymer and associated composite: A review on mechanical properties, defects and treatments. *Polymers*, *12*(7), 1529. http://dx.doi.org/10.3390/polym12071529. PMid:32664374.

Received: Feb. 16, 2021
Revised: June 29, 2021
Accepted: Aug. 27, 2021